Chapter 16

Structure and Properties of Proton Exchange Membrane Fuel Cells at Interfaces

Sangcheol Kim,* Kirt A. Page,* and Christopher L. Soles

Polymers Division, National Institute of Standards and Technology, 100 Bureau Dr, Gaithersburg, MD 20899
***sangcheol.kim@nist.gov; kirt.page@nist.gov**

Although substantial improvements have been demonstrated for fuel cell technology over the past decade, challenges associated with cost and durability need to be overcome to compete in real markets and achieve wide-spread commercial success. Most researchers agree that the catalyst and the membrane are key components for which significant improvement could lead to solutions to these issues. However, as a potential route to solve cost and durability problems, structures and properties at interfaces have not been appropriately understood due to a lack of experimental methods to characterize these complex systems. Recently, in an effort to understand the transport and structural properties of the triple phase interfaces within polyelectrolyte membrane (PEM) fuel cells, thin PEM films cast on flat substrates have been investigated with a variety of techniques to understand the structure and transport at vapor and catalyst surfaces. Since fuel cells are highly integrated systems of heterogeneous materials, the structure and activity at the various interfaces affect the overall performance as much as the individual components. In this review, we review recent efforts to measure structures and physical properties not only at the bulk PEM surface, but also at the heterogeneous interfaces found within the catalyst layers. To overcome longstanding experimental limitations, neutron reflectometry has been deomonstrated as a powerful tool to probe the buried interfacial structure of the PEM within the catalyst layer.

In Polymers for Energy Storage and Delivery: Polyelectrolytes for Batteries and Fuel Cells; Page, K., et al.; ACS Symposium Series; American Chemical Society: Washington, DC, 2012.

Introduction

Since their first emergence as auxiliary power sources in the Gemini space flights, proton exchange membrane fuel cells (PEMFCs) have shown promise due to high efficiency in a wide range of applications such as transportation, stationary and portable power generation. Although substantial improvements in performance have been realized over the past decades, PEMFCs need to overcome two key challenges, cost and durability, to achieve wide-spread commercial success (*1*). The membrane electrode assembly (MEA) is central component of PEMFC and consists of several layers including: a proton exchange or polyelectrolyte membrane (PEM), triple phase anode and cathode catalyst layers, two gas diffusion layers (GDLs), and two sets of sealing gaskets. Generally, the catalyst loaded electrodes are put onto each side of a proton exchange membrane and hot pressed at 111 °C at 3.45 MPa for (2 to 3) minutes. Platinum is the typical catalyst for both the anode and the cathode and is dispersed as (5 to 20) nm particles supported on porous and conductive carbon supports. These porous layers conduct protons to the PEM to complete the ionic path while the electrons move through the conductive carbon to complete the fuel cell circuit. It is important that these layers have optimized transport of gases, water/ions, and electrons in such a way that resistive losses are reduced for the overall fuel cell performance. At high production volumes, the catalyst ink account for nearly half of the fuel cell stack cost due to the expensive platinum (Pt) particles. Another contributor to the cost is the proton exchange membrane, especially at low production volumes. The term "triple phase" means that all of these transport media need to be intimately interfaced at the catalytically active sites. Managing the interfaces of these different phases is extremely important for the ultimate performance of the fuel cell, as well as the overall cost of the system.

Among the many polymeric materials that have been developed for PEMFCs, Nafion (*2*) remains the most suitable membranes due to its thermal stability, chemical stability, and excellent transport properties. Nafion is a copolymer that consists of a polytetrafluoroethylene backbone with randomly distributed perfluorinated-vinyl-polyether side chains terminated with sulfonic acid end groups. In addition to being used as the active PEM material, Nafion is also integrated into the catalyst layers as a binder in the composite structure of carbon supported Pt catalyst particles. As ions must be able to reach the Pt catalyst particles, it is critical that the binder also be an ion conductor. The use of Nafion in the catalyst layer was pioneered by researchers at Los Alamos National Laboratory (*3*, *4*). While early PEM fuel cells required electrodes containing a high platinum loading (4 mg/cm^2) for a high level of performance, Srinivasan *et al.* (*3*) impregnated Nafion into the porous gas diffusion electrode structure and reduced platinum loading by a order of magnitude (to 0.35 mg Pt/cm^2). The reduction of the Pt loading was achieved mainly by extending the three-dimensional reaction zone and optimizing the amount of Nafion impregnated into the electrode structure (*4*). This technical break-through is one of the events that led to the renaissance in PEMFC research over the last 15 years.

For protonic conduction to occur, it is essential that the Nafion be hydrated. It is generally accepted that the kinetics of water transport in Nafion reliably

In Polymers for Energy Storage and Delivery: Polyelectrolytes for Batteries and Fuel Cells; Page, K., et al.; ACS Symposium Series; American Chemical Society: Washington, DC, 2012.

reflects the protonic conductivity which occurs via an aqueous enviroment. There have, however, been several fundamental studies of water diffusion in Nafion membranes under different conditions and the results are generally all over the map. This is because the water transport kinetics are a function of several factors including temperature, membrane water content, the processing condtions for creating the Nafion film, and even the membrane thickness. There are well documented changes in the water diffusion coefficients for Nafion films in the thickness range of (50 to 250) μm, length scale at which finite size effects are generally not observed (*5–7*). Clearly the water and proton transport processes in Nafion are very complicated. The need for high power and energy density is pushing the industry towards thinner membranes in order to reduce the impedance of the fuel cell. As the membrane become increasingly thinner, the mass transport properties across the membrane are more strongly dominated by the interfacial resistance. It was recently suggested that, in a thin PEM, the interfacial resistance could be responsible for a significant portion of the net water transport (*8–11*) and that a less water permeable skin might be formed at the interface (*12*). As the membrane is cast in a very thin film, phase separation of the polymer electrolyte is limited and the interaction with the substrate is significant (*13*)(*14*). This in turn can affect the water content and transport properties of the membrane.

The role of interfacial properties becomes even more dominant in the MEA and with the large quantity of interfaces between the heterogeneous materials. In the composite anodes and cathodes where Nafion is used as a binder, the thickness of the Nafion coatings that actually hold the particles together is on the order of tens of nanometers. In this region, all of the Nafion can be classified as "interfacial" and bulk properties are meaningless. There is a strong need to understand the interplay between components and how the interactions and interfaces between these components affect the transport properties and performance of the fuel cell system. For instance, in the anode, the catalyst particles must participate in three transport functions: (1) adsorbing molecular hydrogen, (2) conducting electrons to the electrode via the catalyst support, and (3) transport of protons into the PEM. Within the catalyst layers, such electrochemical and electrocatalytic processes are most likely affected by the reactions occurring at the triple phase interface consisting of the PEM, vapor, and catalyst surface. To date, a complete understanding of the structures and transport properties at the PEM/metal interface does not exist. However, since impregnated Nafion was shown to significantly enhance the methanol electro-oxidation reaction (*15*), hydrogen anodic oxidation (*15*) and oxygen cathodic reduction reaction (*16–18*) over the bare Pt electrodes, it can be concluded that Nafion strongly interacts with Pt surface and modifies the interfacial properties (*19*, *20*). Difficulty of understanding the true nature of such interfaces has been attributed to a lack of experimental methods for preparing and characterizing well-defined triple phase interface-like systems for electrochemical studies.

Here, we review recent efforts to investigate molecular phenomena and structures not only at the bulk PEM surface but also at the heterogeneous interfaces within the catalyst layers. To overcome longstanding experimental limitations, we discuss in more detail a promising approach using neutron reflectivity which can probe the buried interfaces within the thin film at nanoscale. Understanding

In Polymers for Energy Storage and Delivery: Polyelectrolytes for Batteries and Fuel Cells; Page, K., et al.;
ACS Symposium Series; American Chemical Society: Washington, DC, 2012.

the interfacial structure of the PEM within the catalyst layer is important for shedding light on water transport, proton transport and the oxygen reduction reaction mechanism occurring at the triple-phase interface.

Interfacial Structures and Transport Properties in PEMFC

Interfacial Phenomena in PEM

Over a century ago, von Schroeder (*21*) observed that gelatins would absorb more water under liquid immersion as compared to under 100 % relative humidity (RH) at the same temperature. This phenomenon, which appears to violate the laws of thermodynamics, is now commonly referred to Schroeder's Paradox. While the basis for these observations remains controversial, the explainations typically invoke a structure or phenomenon at the surface of the absorbing material which is different from that of the bulk. Similar observations of Schroeder's Paradox have been reported in the general class of polyelectrolyte membranes that are used for fuel cell applications. A better understanding of the interfacial phenomena in Nafion and Nafion-like materials is of significant importance to the fuel cell membrane community. Reports of this paradox in Nafion have led to fundamental questions about the nature of the interfacial thermodynamics and molecular structure of the material and how they affect the transport properties at the interface with water vapor or with liquid water.

Early AFM work by McLean *et al.* (*22*) suggested that the surface of Nafion is enriched by a thin fluorine rich layer which would seemingly be a barrier to moisture absorption. However X-ray photoelectron spectroscopy (XPS) and dynamic water contact angle measurements by Kim *et al.* (*23*) reported that the surface composition changes upon exposure to liquid water. It was Weber *et al.* (*24*) who first suggested that the surface composition of Nafion could have a major impact on the transport of water through Nafion membranes. While the structure of bulk Nafion is still debated, Weber and coworkers invoked the modified cluster-network model where ionic clusters are connected by hydrophobic channels that have different properties depending of the state of the water in contact with the membrane. They suggested that the surface of Nafion membranes reorganizes from hydrophobic fluorocarbon-rich skin under dry conditions to a hydrophilic sulfonic acid-rich surface in the presence of water.

Majsztrik *et al.* (*12*) argued that water permeation and sorption for thin Nafion membranes at low temperature are controlled by interfacial mass transport at the membrane/air interface. When water vapor is present at both interfaces, the water transport is governed by diffusion kinetics through the membrane. But, the rate-limiting step becomes interfacial transport at the vapor/membrane interface when liquid water is present at just one interface (*25*). This phenomenon was pursued further by Goswami *et al.* (*26*) with advancing and receding contact angle measurements on Nafion and Teflon films. Teflon showed an advancing contact angle of 110° and a receding contact angle of 95°, demonstrating a nonwetting surface for water. In contrast, the receding contact angle on Nafion was between 20° and 30° while the advancing contact angle was 105° to 110°, comparable to the Teflon surface. They attributed this unusual behavior of

In Polymers for Energy Storage and Delivery: Polyelectrolytes for Batteries and Fuel Cells; Page, K., et al.; ACS Symposium Series; American Chemical Society: Washington, DC, 2012.

Nafion to molecular rearrangements at the polymer-fluid interface. The authors, however, were not able to probe how deep below the surface this structural rearrangement occurs. This concept of dynamic rearrangement near the surface was recently explored using water contact angle measurements, AFM and *in-situ* grazing-incidence small-angle X-ray scattering (GI-SAXS) of Nafion under wet and humid conditions (*27*). These measurements showed preferential alignment of micellar-like structures near the interface. The advancing contact angle measured in Figure 1 shows that the Nafion surface is hydrophobic under water vapor but becomes hydrophilic under water immersion. These authors also characterized the Nafion surface after water exposure with AFM and found that the surface roughness increases significantly (Figure 1). The rougher surface topography demonstrates drastic structural variations, which is consistent with the proposed liquid-induced restructuring. These studies are discussed in detail in the chapter entitled "Thermodynamics, microstructure and interfacial effects in hydrated Nafion" of this book.

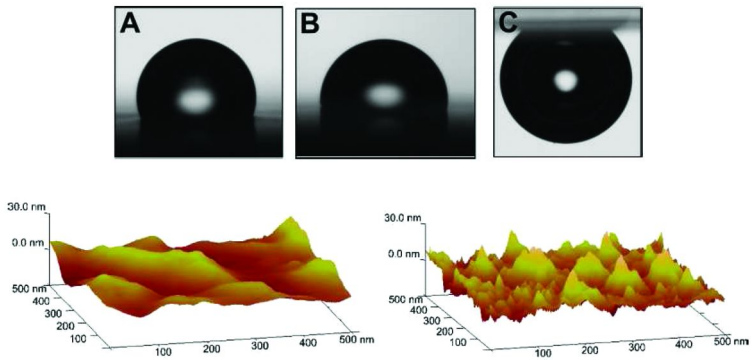

Figure 1. Water droplets in air on Nafion, dry film (upper left) and equilibrated at RH = 97 % (upper middle), and air bubble attached from below Nafion in water (upper right). Surface topography of Nafion measured by AFM in air (lower left) and under water (lower right). Reprinted with permission from (27) © 2010 American Chemical Society.

Zhao and co-workers (*28*) used pulse field gradient spin echo nuclear magnetic resonance (PGSE-NMR) to quanitify self-diffusion coefficient of water within a Nafion membrane and interpreted their findings in terms of the tortuosity of the hydrophilic water conduction channels. They argue that surface energy is minimized by having the water transport channels buried beneath the surface in geometries that are non-conductive for interfacial transport when the membrane surface is in contact with a water vapor. However, these water transport channels extend directly to the interface when the Nafion is in contact with liquid water. Their interpretation of the NMR data is consistent with the notion that the nanophase-separated structure of Nafion, driven by the hydrophilic side-chain segregation from the hydrophobic backbone, is responsible for its complex interfacial transport behaviors. To date, however, a clear molecular-level understanding of interfacial mass transport resistance has not emerged. For

In Polymers for Energy Storage and Delivery: Polyelectrolytes for Batteries and Fuel Cells; Page, K., et al.; ACS Symposium Series; American Chemical Society: Washington, DC, 2012.

example, there has been no determination of the length scale over which the interfacial resistance persists. This can only be determined from a detailed molecular-level understanding of this phenomenon.

Interfacial Phenomena in MEA

As the polymer electrolyte membrane material is also used as an active binder in the electrode catalyst layers, the nature of the triple phase interface between heterogeneous materials needs to be well understood. However, it is very difficult to measure or quantify these interfaces especially when the Pt catalyst is usually a nanoparticle, the electron conductor is a combination of graphitic or nanofiber form of carbon and the Nafion binder is a poorly defined layer holding these components together. Due to such a complicated and poorly defined geometry, it is difficult to describe accurately the molecular-level structure of the triple phase interface and its effect on electrochemical processes. The measurements are just too complicated. To simplify the situation, researchers have started to utilize model thin PEM films cast on flat substrates. This approach has made it much easier to quantify the role of the interfaces; thin film measurements are relatively well established.

Pt is the most common catalyst for the oxygen reduction in a hydrogen fuel cell and there have been several attempts to indentify this reaction mechanism on model planar Pt interfaces using both electrochemical X-ray photoelectron spectroscopy (EC-XPS) (*29*), which has high sensitivity and specificity of the O_{1s} spectra, and *in-situ* attenuated total reflectance-Fourier transform infrared (ATR-FTIR) (*30*). There are also recent reports of utilizing half-membrane-electrode assembly type cells by Kunimatsu *et al.* (*31*) to conduct ATR-FTIR measurements at the Pt/Nafion interface under humidified N_2/O_2 atmosphere. An infrared absorption band observed near 1400 cm^{-1} to 1403 cm^{-1} under humidified oxygen atmosphere is assigned as the O-O vibration of the adsorbed oxygen molecule O_2.

There have also been attempts to develop a molecular-level structural description of the triple phase interface through a combination of *in-situ* infrared reflection absorption spectroscopy (IRRAS) and cyclic voltammetry on model Pt(111)/Nafion interfaces in $HClO_4$ acid solutions (*32*). Analysis of the infrared data revealed that proton mobility inside the membrane is enhanced with the deprotonation of sulfonic groups near the electrode surface in the presence of higher potentials. The authors attributed this effect to an electric field induced orientation of the membrane morphology. They also observed that the character of CO absorption and oxidation at Pt(111) is affected by the presence of polymer electrolyte membrane. The nature of the Pt-Nafion interface for both polycrystalline and single crystal Pt surfaces was probed by Subbaraman *et al.* (*33*) using a voltammetric fingerprinting approach. A CO charge displacement technique identified that the sulfonate anions of Nafion adsorb onto the Pt surface. They report that the nature and strength of the adsorption is significantly influenced by the presence of the native interactions of these anions with their host polymer matrix. The adsorption behavior of the sulfonate anions at the interface is consistent with the elucidation by the cooperative efforts using *operando*

In Polymers for Energy Storage and Delivery: Polyelectrolytes for Batteries and Fuel Cells; Page, K., et al.;
ACS Symposium Series; American Chemical Society: Washington, DC, 2012.

(actual reactor conditions) infrared (IR) spectroscopy, polarization modulated IR spectroscopy (PM-IRRAS) of Nafion-Pt interfaces, ATR-FTIR spectroscopy of bulk Nafion, and density functional theory (DFT) calculations of the resulting spectra (*34*). As illustrated in Figure 2, sulfonate and CF_3 co-adsorbates of the Nafion side chain are anchored at the Nafion-Pt interface and reduce the degrees of freedom available for backbone and side chain dynamics. Such adsorption partially orders the Nafion backbone and/or side-chain CF_2 groups relative to the Pt surface.

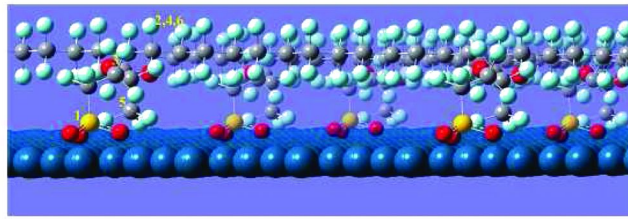

Figure 2. A model for Nafion functional group adsorption to Pt: carbon (gray), fluorine (light blue), sulfur (yellow), oxygen (red), and Pt (dark blue) (color online). Reprinted with permission from (34) © 2010 American Chemical Society.

Quartz-crystal microbalance (QCM) measurements have been used to quantify the water content (λ) of thin Nafion membranes (0.033 μm to 3 μm thick) on Pt substrates over a range of temperatures and and relative humidities (RHs) (*35*). For films down to approximately 500 nm, the measured water uptakes are very similar to that of a thick Nafion membrane. However, when the thickness drops below 33 nm, these measurements indicate that the membrane water content is slightly reduced, especially at higher vapor water activities. These authors speculate that the lower water content results from either interactions of the ionomers with the substrate, surface confinement, or a water-impermeable layer at the gas/ionomer interface. Their observations did not appear to depend on specific substrate-ionomer interactions as identical results were obtained on both Au-coated and Pt-coated quartz crystals.

Molecular simulations to characterize the structure and dynamics of the processes at Nafion interfaces have the potential to provide new insights into the electrochemical processes within the catalyst layers. Selvan *et al.* (*36*) performed molecular dynamics (MD) simulations and observed a region of water depletion in Nafion membrane near the vapor interface. They concluded that there is no additional resistance to mass transport of the vehicular component of water and hydronium due to the interface. However, there is a decrease in the fraction of fully hydrated hydronium ions at the interface. MD simulations were also performed by Liu *et al.* (*37*) to investigate the structural and dynamical behavior of water and hydronium ions at the electrode/electrolyte interface in PEMFCs. As shown in Figure 3, they observed significant wetting of the catalyst surface (Pt(111)) and no wetting of the catalyst support surface (graphite). The degree of wetting depended strongly on the level of the water content. However, no more than a monolayer of surface structure was observed. This monolayer was

In Polymers for Energy Storage and Delivery: Polyelectrolytes for Batteries and Fuel Cells; Page, K., et al.; ACS Symposium Series; American Chemical Society: Washington, DC, 2012.

composed of a mixture of water, Nafion, and hydronium ions. Because the catalyst support shows no significant wetting, this work implies that the catalyst particles must be in intimate contact with the hydrated membrane, or with recast hydrated polymer electrolyte membrane in the electrode that provides a pathway for protons to move from the catalyst surface into the bulk hydrated membrane.

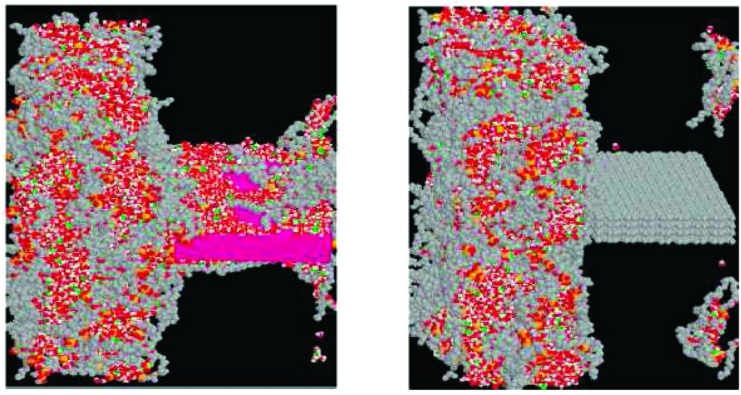

Figure 3. Final snapshots of simulations containing the Pt catalyst surface (left) and the carbon catalyst support surface (right) for water contents of 20 % by mass: CF_x groups (gray), sulfur (orange), oxygen of H_2O and SO_3^- (red), oxygen of H_3O^+ (green), hydrogen (white), Pt (pink), and graphitic carbon (gray) (color online). Reprinted with permission from (37) © 2008 American Chemical Society.

Interfacial Structure Characterization in MEA

While interfacial phenomena are commonly invoked to describe an unusual response or performance of fuel cell membranes, there have been relatively few studies that directly correlate this response to an actual interfacial structure. This is in part because such interfacially selective measurements have been difficult, especially with the added complexity that the bulk structure of PEMs like Nafion are still debated. However, there appears now an increasing number of reports in the literature that directly address this interfacial structure issue. In this section we review several of these recent advances.

Neutron reflectivity (NR) and X-ray reflectivity (XR) are powerful tools to characterize swelling dynamics and distribution of water at interfaces and in thin films (*38–41*). For details on the NR technique, please refer to the chapter entitled "In situ neutron techniques for studying lithium ion batteries" in this book. Some early examples illustrate how NR can be used to quantify the equilibrium concentration of water at the buried interfaces between an amorphous polyimide film and silicon substrate. These measurements showed an excess of water, dependent upon the substrate hydrophilicity, at the polymer/substrate interfaces (*38*, *39*). This excess of interfacial moisture in a polymer film on a hydrophilic substrate is manifest through an increased degree of swelling

In Polymers for Energy Storage and Delivery: Polyelectrolytes for Batteries and Fuel Cells; Page, K., et al.; ACS Symposium Series; American Chemical Society: Washington, DC, 2012.

of the entire film when the film thickness approaches the length scale of the interfacial enhancement: this effect nominally becomes visible for films thinner than approximtately 50 nm (*40*). It was further shown that this interfacial uptake could be reduced by making the substrate interface more hydrophobic than the polymer film (*42*). These authors coupled these interfacial moisture absorption studies with *in-situ* QCM measurements that demonstrated significantly reduced uptake kinetics in both thin polymer (*42*) and polyelectroyte films (*43*).

There have been attempts to perform *in-situ* NR measurements of water penetration into thin sulfonated polyphenylene (sPP) ionomer films as a function of time, ionic strength, and film thickness (*44*). NR measurements are typically too slow to track the swelling response of a thin film *in-situ*, so these authors focused on fiting only the low *q* data of the reflectivity curve (where counting statistics are higher) to acquire partial curves. sPP films with an initial thicknesses of 131 Å, 218 Å and 567 Å with 33.4 % sulfonation were exposed to D_2O vapors and subsequently measured by NR in time-averaged 10 min intervals. The data were analyzed by fitting a 3-layer model as illustrated in Figure 4. The scattering length density (SLD) is profiled as a function of the distance (Z) from Si substrate. At steady state, nonuniform distributions of water molecules were observed with D_2O-rich layers (higher SLD) at the both air/polymer interface and polymer/SiO_x substrate interface. The formation of a thin water-rich layer is somewhat unusual since the hydrophobic thin layer is preferred at the air interface, especially in case of fluorinated ionomers (e.g., Nafion) (*45*). Generally, the lower surface tension component tends to segregate predominantly to the air interface for the lowest energy configuration. However, the authors speculated that the rigidity of the sPP backbone may not be sufficient to allow chain folding to bury the ionic groups. Figure 4 also suggests that a water rich interface exists near the SiO_x substrate in the 131 Å thick film, but for some reason this preferential accumulation is lost for the 567 Å thick film. It is not immediately clear why this preferential accumulation would disappear in the thicker film, but it needs to be noted that film thickness, roughness, and SLD become highly convoluted when fitting NR data for films on the order of 131 Å. By only fitting the low *q* data the authors would not be able to separate these effects for their thinnest films.

Wood and coworkers (*14*) also used NR to characterize the interfacial morphology of Nafion on smooth and idealized glassy carbon (GC) substrates coated with device relevant Pt or Pt oxide (PtO) layers. The spin cast Nafion films were thermally processed following the electrode preparation method developed by Wilson and Gottesfeld (*46*, *47*). It resulted in Nafion films on top of either hydrophobic Pt or hydrophilic PtO substrates. When the Nafion was equilibrated with saturated D_2O on the Pt surface, the best fit to the data (Figure 5) showed a dip in the SLD profile near the hydrophobic substrate: a thin water depletion region (SLD = 4.6×10^{-6} Å^{-2}, thickness = 74 Å) beneath a thicker hydrated (SLD = 5.1×10^{-6} Å^{-2}, thickness = 619 Å) layer of Nafion. After conversion of the Pt surface to PtO, the interfacial depletion region disappeared and the resulting hydrated film could be modeled with a bilayer structure. In this bilayer, the Nafion adjacent the hydrophilic PtO absorbed more D_2O (SLD = 5.0×10^{-6} Å^{-2}, thickness = 372 Å) while the Nafion adjacent to the air interface is comparatively more hydrophobic layer (SLD = 4.7×10^{-6} Å^{-2} thickness = 333 Å).

In Polymers for Energy Storage and Delivery: Polyelectrolytes for Batteries and Fuel Cells; Page, K., et al.; ACS Symposium Series; American Chemical Society: Washington, DC, 2012.

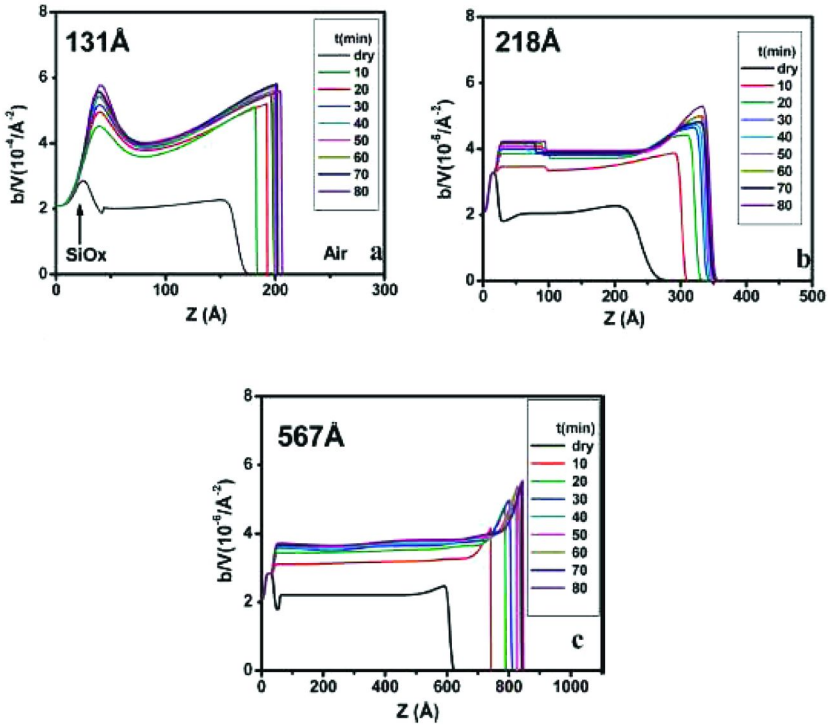

Figure 4. NR Scattering length density profiles of sPP thin films with initial thickness of 131 Å (upper left), 218 Å (upper right), and 567 Å (lower) as a function of exposure time to D_2O vapor. Z is the distance from Si substrate at Z = 0. Reprinted with permission from (44) © 2008 American Chemical Society.

Reversible restructuring of Nafion morphology at the interface with Pt was previously proposed by ultramicroelectrode studies. When Nafion is in contact with a bare Pt surface, the hydrophilic sulfonate-containing side chains are driven away from the hydrophobic Pt surface. When the Pt surface becomes hydrophilic PtO, the sulfonate-containing side chains are drawn back into the interface, leaving hydrophobic fluorinated segments at the surface. While the NR data presented above seem to support this general picture, it is hard to imagine how such a phase segregation of the different domains could occur for a random copolymer like Nafion over length scales as large as 600 Å to 700 Å: the short-range average distance between the different segments in a polymer chain would seemingly prevent phase demixing at such large length scale. Furthermore, this proposed surface templating effect is inconsistent with other interpretations that Nafion is anchored onto the Pt surface using sulfonate anion groups (*33*, *35–37*). The nature of the interfacial interactions between Pt, PtO, and Nafion are clearly very complicated.

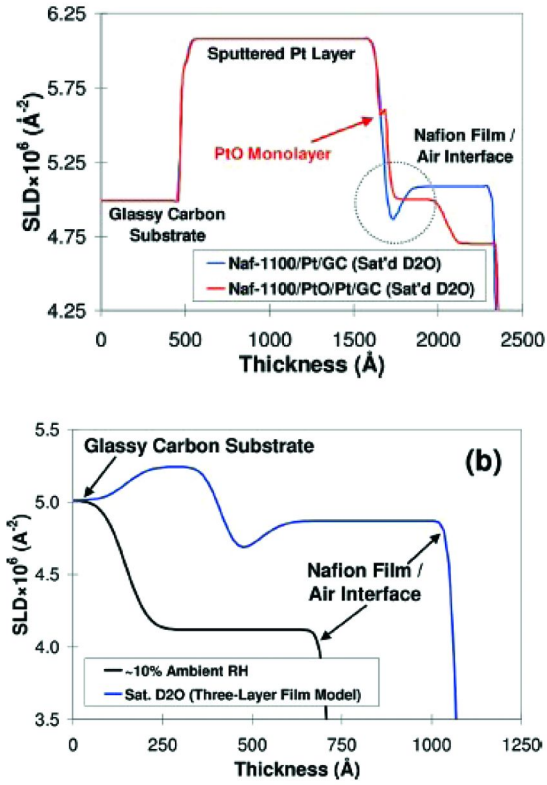

Figure 5. NR scattering length density (SLD) profiles of Nafion: on Pt surface or PtO surface in a saturated D_2O environment (upper); on glassy carbon surface in saturated D_2O and ambient 10 % RH environments (lower). Reprinted with permission from (14) © 2009 American Chemical Society.

When the Nafion film on GC surface was measured in a saturated D_2O environment, different multilayer structures of Nafion were found. As shown in Figure 5, reasonable agreement is achieved by three-layer heterogeneous model consisting of a thin, rough intermediate "more hydrophobic" zone between two thicker, more hydrophilic layers. Like Nafion on the Pt surface, the thickest hydrophilic layer existes at the air interface. However, the most hydrophilic layer is additionally found at the GC interface and the total thickness of the three zones increased nearly 60 %. These results are in contradiction to what Liu *et al.* (*37*) observed with molecular dynamics simulations and the structural rearrangement of Nafion surface proposed by Bass *et al.* (*27*) as a extension of Schroeder's Paradox.

NR was also used by Dura and coworkers (*13*) to demonstrate that lamellar layers of thin alternating water-rich and Nafion-rich domains are induced at the interface of hydrated Nafion with native Si oxide substrates. Nafion solution were spin cast onto various substrates and then immediately annealed at either 60 °C or

In Polymers for Energy Storage and Delivery: Polyelectrolytes for Batteries and Fuel Cells; Page, K., et al.;
ACS Symposium Series; American Chemical Society: Washington, DC, 2012.

150 °C for 1 h. As shown in Figure 6a, the Nafion spin-cast onto SiO_2 shows a peak at $Q_z = 0.21$ Å^{-1} at RH = 97 %. The position and intensity of the peak are strongly dependent on sample hydration level, which suggests that water is inducing the structure. Transverse scans to probe the in-plane structure suggest that the high-Q peak stems from extended two-dimensional planes or lamellae running parallel to the substrate. The best fit SLD profiles to the experimental data are presented in Figure 6b and show excellent agreement with the specular reflectivity data. The cartoon schematic in Figure 6b illustrates corresponding layer structures. For Nafion on SiO_2 at RH=97 %, the layers in the model correspond to the Si substrate, the native Si oxide layer, and then the lamellae consisting of three water-rich layers alternating with two Nafion-rich layers. The composition of the lamellae decayed from nearly 100 % by volume H_2O to a final layer of ≈ 60 % by volume H_2O with increasing distance from the interface. The "bulk" layer on top of the lamellae is consistent with Nafion that has a water content (λ) of (5.0 ± 0.2) water molecules per sulfonic acid. Upon dehydration, as shown in Figure 6b (green), the lamellar structure has been reduced in extent and only three layers are observed. It is notable that this interfacial lamellar structure is not observed for the Nafion/Pt or Nafion/Au interfaces except a thin partially hydrated single interfacial layer. But, the thickness decreases to a few Å as humidity is reduced to zero. This indicates that Au and Pt surfaces have a lower affinity for the sulfonic acid of Nafion/water phase than the more hydrophilic SiO_2 surface.

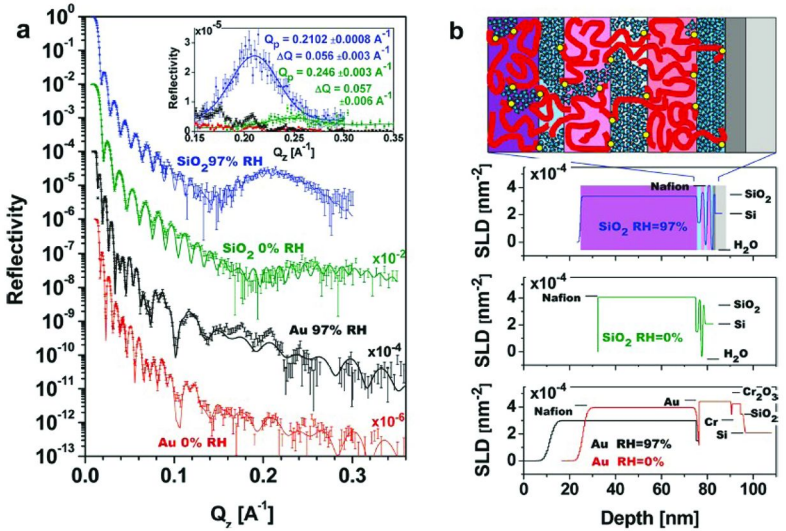

Figure 6. (left) Specular NR data and model fits showing a high-Q peak for SiO_2 at RH = 97 % (blue), a smaller high-Q peak for SiO_2 at RH = 0 % (green) and no high-Q peak for Au at RH =97 % (black) or Au at RH = 0 % (red). (right) NR scattering length density profiles and the model corresponding to SiO_2 at RH =97 %: Nafion fluorocarbon backbone (red), sulfonic acid group (yellow), and water (blue) (color online). Reprinted with permission from (13) © 2009 American Chemical Society.

In Polymers for Energy Storage and Delivery: Polyelectrolytes for Batteries and Fuel Cells; Page, K., et al.; ACS Symposium Series; American Chemical Society: Washington, DC, 2012.

Currently, we are investigating the origins of the interfacial lamellar formation and its impact on transport properties using NR, GISAXS, and QCM. Our approach has been to measure the structure and transport properties of Nafion thin films spin cast onto model substrates having various surface energies (*48*). The interfacial structures of Nafion and water appears to be strongly dependent on the surface energy of the substrate. We generally do not observe interfacial lamella in hydrdated Nafion cast on hydrophobic surfaces. However, strongly hydrophilic surface tend to show interfacial lamella formation for fully hydrated Nafion films. These results seem reasonably consistent with previous observations of wetting on catatlyst layer surfaces (*37*) and an excess of water at the interfaces of polymers with hydrophilic surfaces (*38–40*, *42–44*). Our systematic approach can give an insight into the premature but controversial debates on the interfacial Nafion behavior as discussed above.

Summary and Outlook

To be competitive in commercial markets, fuel cells technology should overcome technical challenges associated with cost and durability. The catalyst ink account for nearly half of the fuel cell stack cost due to the expensive Pt particles. Another major contributor to the cost is the proton exchange membrane. Most researchers agree that the catalyst and the membrane are key components for which significant improvement could lead to a solution to these issues. Although impressive advances on individual components have been achieved, the importance of understanding the interfaces has not been adequately addressed. Since the fuel cell is a highly integrated system of heterogeneous materials, the structure and (transport) activity at the interface affect the overall performance as much as the individual components. Innovations in the characterization and analysis techniques aimed at improving our understanding of the electrochemical processes, the structure and the transport at interfaces present in PEMFCs have been developed and are hoped to make efficient progress in eliminating cost and durability challenges that the current fuel cell technology faces. In this review, we introduced recent efforts to investigate structures and properties not only at the PEM interface but also at the heterogeneous interfaces within the catalyst layers.

References

1. Martin, K. E.; Kopasz, J. P.; McMurphy, K. W. Fuel Cell Chemistry and Operation. *ACS Symp. Ser.* **2010**, *1040*, 1–13.
2. Certain commercial equipment, i., or materials are identified in this paper in order to specify the experimental procedure adequately. Such identification is not intended to imply recommendation or endorsement by the National Institute of Standards and Technology, nor is it intended to imply that the materials or equipment identified are necessarily the best available for the purpose.
3. Ticianelli, E. A.; Derouin, C. R.; Redondo, A.; Srinivasan, S. *J. Electrochem. Soc.* **1988**, *135*, 2209–2214.

In Polymers for Energy Storage and Delivery: Polyelectrolytes for Batteries and Fuel Cells; Page, K., et al.; ACS Symposium Series; American Chemical Society: Washington, DC, 2012.

4. Paik, W.; Springer, T. E.; Srinivasan, S. *J. Electrochem. Soc.* **1989**, *136*, 644–649.
5. Zawodzinski, T. A.; Neeman, M.; Sillerud, L. O.; Gottesfeld, S. *J. Phys. Chem.* **1991**, *95*, 6040–6044.
6. Rivin, D.; Kendrick, C. E.; Gibson, P. W.; Schneider, N. S. *Polymer* **2001**, *42*, 623–635.
7. Burnett, D. J.; Garcia, A. R.; Thielmann, F. *J. Power Sources* **2006**, *160*, 426–430.
8. Satterfield, M. B.; Benziger, J. B. *J. Phys. Chem. B* **2008**, *112*, 3693–3704.
9. Merida, W.; Romero, T. *J. Membr. Sci.* **2009**, *338*, 135–144.
10. Navessin, T.; Adachi, M.; Xie, Z.; Li, F. H.; Tanaka, S.; Holdcroft, S. *J. Membr. Sci.* **2010**, *364*, 183–193.
11. Tabuchi, Y.; Ito, R.; Tsushima, S.; Hirai, S. *J. Power Sources* **2011**, *196*, 652–658.
12. Majsztrik, P. W.; Satterfield, M. B.; Bocarsly, A. B.; Benziger, J. B. *J. Membr. Sci.* **2007**, *301*, 93–106.
13. Dura, J. A.; Murthi, V. S.; Hartman, M.; Satija, S. K.; Majkrzak, C. F. *Macromolecules* **2009**, *42*, 4769–4774.
14. Wood, D. L.; Chlistunoff, J.; Majewski, J.; Borup, R. L. *J. Am. Chem. Soc.* **2009**, *131*, 18096–18104.
15. Maruyama, J.; Inaba, M.; Katakura, K.; Ogumi, Z.; Takehara, Z. *J. Electroanal. Chem.* **1998**, *447*, 201–209.
16. Gottesfeld, S.; Raistrick, I. D.; Srinivasan, S. *J. Electrochem. Soc.* **1987**, *134*, 1455–1462.
17. Floriano, J. B.; Ticianelli, E. A.; Gonzalez, E. R. *J. Electroanal. Chem.* **1994**, *367*, 157–164.
18. Watanabe, M.; Miyatake, K.; Omata, T.; Tryk, D. A.; Uchida, H. *J. Phys. Chem. C* **2009**, *113*, 7772–7778.
19. Watanabe, M.; Yano, H.; Higuchi, E.; Uchida, H. *J. Phys. Chem. B* **2006**, *110*, 16544–16549.
20. Ohma, A.; Fushinobu, K.; Okazaki, K. *Electrochim. Acta* **2010**, *55*, 8829–8838.
21. von Schroeder, P. *Z. Phys. Chem.-Stoch. Ve* **1903**, *45*, 75–117.
22. McLean, R. S.; Doyle, M.; Sauer, B. B. *Macromolecules* **2000**, *33*, 6541–6550.
23. Kim, Y. H.; Oblas, D.; Angelopoulos, A. P.; Fossey, S. A.; Matienzo, L. J. *Macromolecules* **2001**, *34*, 7489–7495.
24. Weber, A. Z.; Newman, J. *J. Electrochem. Soc.* **2003**, *150*, A1008–A1015.
25. Majsztrik, P.; Bocarsly, A.; Benziger, J. *J. Phys. Chem. B* **2008**, *112*, 16280–16289.
26. Goswami, S.; Klaus, S.; Benziger, J. *Langmuir* **2008**, *24*, 8627–8633.
27. Bass, M.; Berman, A.; Singh, A.; Konovalov, O.; Freger, V. *J. Phys. Chem. B* **2010**, *114*, 3784–3790.
28. Zhao, Q. A.; Majsztrik, P.; Benziger, J. *J. Phys. Chem. B* **2011**, *115*, 2717–2727.
29. Wakisaka, M.; Suzuki, H.; Mitsui, S.; Uchida, H.; Watanabe, M. *J. Phys. Chem. C* **2008**, *112*, 2750–2755.

In Polymers for Energy Storage and Delivery: Polyelectrolytes for Batteries and Fuel Cells; Page, K., et al.; ACS Symposium Series; American Chemical Society: Washington, DC, 2012.

30. Shao, M. H.; Liu, P.; Adzic, R. R. *J. Am. Chem. Soc.* **2006**, *128*, 7408–7409.
31. Kunimatsu, K.; Yoda, T.; Tryk, D. A.; Uchida, H.; Watanabe, M. *Phys. Chem. Chem. Phys.* **2010**, *12*, 621–629.
32. Gomez-Marin, A. M.; Berna, A.; Feliu, J. M. *J. Phys. Chem. C* **2010**, *114*, 20130–20140.
33. Subbaraman, R.; Strmcnik, D.; Stamenkovic, V.; Markovic, N. M. *J. Phys. Chem. C* **2010**, *114*, 8414–8422.
34. Kendrick, I.; Kumari, D.; Yakaboski, A.; Dimakis, N.; Smotkin, E. S. *J. Am. Chem. Soc.* **2010**, *132*, 17611–17616.
35. Kongkanand, A. *J. Phys. Chem. C* **2011**, *115*, 11318–11325.
36. Selvan, M. E.; Liu, J.; Keffer, D. J.; Cui, S.; Edwards, B. J.; Steele, W. V. *J. Phys. Chem. C* **2008**, *112*, 1975–1984.
37. Liu, J. W.; Selvan, M. E.; Cui, S.; Edwards, B. J.; Keffer, D. J.; Steele, W. V. *J. Phys. Chem. C* **2008**, *112*, 1985–1993.
38. Wu, W. L.; Orts, W. J.; Majkrzak, C. J.; Hunston, D. L. *Polym. Eng. Sci.* **1995**, *35*, 1000–1004.
39. Tan, N. C. B.; Wu, W. L.; Wallace, W. E.; Davis, G. T. *J. Polym. Sci., Polym. Phys.* **1998**, *36*, 155–162.
40. Vogt, B. D.; Soles, C. L.; Jones, R. L.; Wang, C. Y.; Lin, E. K.; Wu, W. L.; Satija, S. K.; Goldfarb, D. L.; Angelopoulos, M. *Langmuir* **2004**, *20*, 5285–5290.
41. Mukherjee, M.; Singh, A.; Daillant, J.; Menelle, A.; Cousin, F. *Macromolecules* **2007**, *40*, 1073–1080.
42. Vogt, B. D.; Soles, C. L.; Lee, H. J.; Lin, E. K.; Wu, W. *Polymer* **2005**, *46*, 1635–1642.
43. Vogt, B. D.; Soles, C. L.; Lee, H. J.; Lin, E. K.; Wu, W. L. *Langmuir* **2004**, *20*, 1453–1458.
44. He, L. L.; Smith, H. L.; Majewski, J.; Fujimoto, C. H.; Cornelius, C. J.; Perahia, D. *Macromolecules* **2009**, *42*, 5745–5751.
45. Zawodzinski, T. A.; Gottesfeld, S.; Shoichet, S.; Mccarthy, T. J. *J. Appl. Electrochem.* **1993**, *23*, 86–88.
46. Wilson, M. S.; Gottesfeld, S. *J. Appl. Electrochem.* **1992**, *22*, 1–7.
47. Wilson, M. S.; Gottesfeld, S. *J. Electrochem. Soc.* **1992**, *139*, L28–L30.
48. Kim, S.; Dura, J. A.; Page, K. A.; Soles, C. L. *Abstr. Pap., Am. Chem. Soc.* **2011**, *241*.